

# Adaptive Optics Assisted Near-Infrared Spectroscopy of SVS 13 and its Jet<sup>1</sup>

C.J. Davis

*Joint Astronomy Centre, 660 N. A'ohōkū Place, Hilo, Hawaii 96720, USA*

`c.davis@jach.hawaii.edu`

B. Nisini

*INAF-Osservatorio Astronomico di Roma, Via di Frascati 33, I-00040 Monteporzio  
Catone, Italy*

M. Takami and T.-S. Pyo

*Subaru Telescope, 650 N. A'ohōkū Place, Hilo, Hawaii 96720, USA*

M.D. Smith

*Armagh Observatory, College Hill, Armagh, N. Ireland*

E. Whelan and T.P. Ray

*Dublin Inst. Advanced Studies, 5 Merrion Square, Dublin 2, Ireland*

A. Chrysostomou

*Centre for Astrophysics Research, University of Hertfordshire, Hatfield, Herts AL10 9AB,  
UK*

## ABSTRACT

We present long-slit H- and K-band spectroscopy of the low-mass outflow source SVS 13, obtained with the adaptive-optics assisted imager-spectrometer *NACO* on the *VLT*. With a spatial resolution of  $<0.25''$  and a pixel scale of

---

<sup>1</sup>Based on Observations collected at the European Southern Observatory, Paranal, Chile (ESO programmes 074.C-0408).

0.027'' we precisely establish the relative offsets of H<sub>2</sub>, [Fe II], CO, H I and Na I components from the source continuum. The H<sub>2</sub> and [Fe II] peaks are clearly associated with the jet, while the CO, H I and Na I peaks are spatially unresolved and coincident with the source, as is expected for emission associated with accretion processes. The H<sub>2</sub> profile along the slit is resolved into multiple components, which increase in size though decrease in intensity with distance from the source. This trend might be consistent with thermal expansion of packets of gas ejected during periods of increased accretion activity. Indeed, for the brightest component nearest the source, proper motion measurements indicate a tangential velocity of 0.028''/year. It therefore seems unlikely that this emission peak is associated with a stationary zone of warm gas at the base of the jet. However, the same can not be said for the [Fe II] peak, for which we see no evidence for motion downwind, even though radial velocity measurements indicate that the emission is associated with higher jet velocities. We postulate that the [Fe II] could be associated with a collimation shock at the base of the jet.

*Subject headings:* ISM: jets and outflows – ISM: Herbig-Haro Objects – stars: pre-main-sequence – stars: individual (SVS 13)

## 1. Introduction

With high-spectral-resolution observations one may probe emission-line regions at the bases of jets, and thereby hope to distinguish between – or at least constrain – models of jet collimation and acceleration. Indeed, there are a number of diagnostic atomic and molecular lines in the near-infrared (near-IR) that are particularly useful for studying the more deeply embedded Young Stellar Objects (YSOs) (Davis et al. 2001, 2003; Pyo et al. 2002; Whelan et al. 2004; Takami et al. 2005; Nisini et al. 2005). Most notable are the [Fe II] and H<sub>2</sub> lines, which are found to be bright at the base of a number of jets from Class I protostars. The emission is usually blue-shifted, the [Fe II] tracing a higher-velocity component than the H<sub>2</sub>, and offset along the axis of the jet by a few 10s of AU. These two species trace very different flow components: the [Fe II] derives from hot, dense, partially-ionised, gas (T~10,000 K) while the H<sub>2</sub> traces low-excitation, shocked (or possibly fluoresced) molecular gas (T~2,000 K). These forbidden emission line (FEL) and molecular hydrogen emission line (MHEL) regions exist within a few hundred AU of each outflow source, and are therefore either within or very close to the primary jet collimation and acceleration zone. The H<sub>2</sub> may be entrained along the walls of the [Fe II] jet, or it may trace a cooler molecular disk wind ejected at larger disk radii.

As a further step toward a better understanding of these emission-line regions, here we present adaptive-optics (AO) corrected H- and K-band spectra of the MHEL and FEL regions associated with SVS 13, the driving source of the HH 7-11 Herbig-Haro (HH) jet and molecular outflow (Chrysostomou et al. 2000; Bachiller et al. 2000). The source is located in the L 1450 molecular cloud near the active low-mass star forming region NGC 1333 in Perseus. SVS 13 is assumed to be at a distance of 300 pc (Cernis 1990; de Zeeuw et al. 1999); modeling of the HH bow shocks in the flow imply an inclination angle of  $\sim 30^\circ$ - $50^\circ$  with respect to the plane of the sky (Hartigan, Raymond & Hartmann 1987; Smith, Khanzadyan & Davis 2003). The *VLT* observations presented here complement the earlier *U.K. Infrared Telescope (UKIRT)* observations of Davis et al. (2001, 2003), which yielded important kinematic information though lacked spatial resolution, and the more recent *Subaru* observations of Takami et al. (2005), where a thorough excitation analysis has been made.

## 2. Observations

The combination of *NAOS* and *CONICA* at the *European Southern Observatory (ESO)* *Very Large Telescope (VLT)* provides AO correction using an IR-bright guide star in conjunction with near-IR spectroscopy. In our case, the jet source itself, SVS 13 (J $\sim$ 11.6, K $\sim$ 8.1), was used as the AO reference star. The S27-3-SH and S27-3-SK modes used yield a wavelength coverage of 1.37-1.72 $\mu$ m and 2.02-2.53 $\mu$ m at a spectral resolution of R $\sim$ 1500. The slit width was 0.172'', the pixel scale along the slit was 0.0270''( $\pm$ 0.0002'') (measured from the offsets of a bright star along the slit), and the slit length was 28''. The H- and K-band observations were conducted in service mode on 13 and 17 January 2005, respectively. With the slit aligned along the SVS 13 jet axis (position angle = 159° E of N), the telescope was nodded between object and blank sky six times in each waveband. Two 150 sec exposures were obtained at each position.

The individual spectral images were bad-pixel masked and flat-fielded using observations of a halogen lamp. Sky exposures were subtracted from object frames before wavelength calibration using argon arc spectra. *Starlink FIGARO* routines were used to correct for distortion along the slit axis, so that the wavelength calibration was constant along the spatial axis (along columns). The continuum associated with SVS 13 was then registered along the slit axis before co-addition of the data. Individual sky-subtracted images were compared to the shifted and co-added data in each waveband to make sure that the spatial resolution had not been compromised by this shifting and averaging process. From Lorentzian fitting to profiles taken through the SVS 13 continuum at various wavelengths, the full width at half maximum (FWHM) was found to vary between 0.24'' and 0.40'' in H, and 0.19'' and 0.35''

in K; in the averaged data the FWHM was  $0.26''(\pm 0.03'')$  in H and  $0.23''(\pm 0.02'')$  in K.

The B5V bright star HIP 30943 ( $V=8.0$ ) was observed as a telluric standard. However, the extracted H- and K-band spectra of this source contain deep H $\alpha$  brackett absorption lines. Model Vega spectra were therefore used to remove these lines. Briefly, via an iterative process similar to that described by Vacca, Cushing & Rayner (2003), the model data were scaled, smoothed and shifted before division into the HIP 30943 spectra. Comparison of the corrected HIP 30943 spectra with theoretical atmospheric transmission spectra presented by Vacca et al. (2003) showed that this process worked very well; the small difference in spectral type between Vega (A0V) and the standard (B5V) had no noticeable affect on the H $\alpha$  fitting. The atmospheric absorption features remaining in the corrected HIP 30943 spectra were subsequently aligned with equivalent features in the H- and K-band SVS 13 data, before the HIP 30943 spectra were “grown” into spectral images and divided into the SVS 13 spectral images.

### 3. Near-IR spectroscopy

H and K-band spectral images are shown in Figures 1, 2 and 3. To more clearly show the line-emission features, the SVS 13 continuum has been removed from each image, row by row, by fitting a second-order polynomial to wavelength regions free of line emission. However, residual shot noise associated with the bright continuum does remain in some parts of the data.

As is the case in other spectroscopic studies (Davis et al. 2001; Takami et al. 2005), extended emission is observed only in H $_2$ . However, for the first time, faint H $_2$  emission is also observed in the SVS 13 counter-jet (positive offsets in Figure 3). The H $\alpha$  Brackett lines in the H-band, and the CO, Br $\gamma$  and NaI lines in the K-band all appear as compact peaks coincident with the continuum. The [Fe II] peak is also compact, although it is slightly offset along the blue-shifted jet.

In Figure 4 we compare plots of the H $_2$  1-0S(1) and [Fe II]  $1.644 \mu\text{m}$  profiles traced along the slit, together with profiles of the adjacent continuum. The continuum plots are the average of profiles extracted slightly blue-ward and red-ward of the line in each case. The continuum profiles effectively show the spatial resolution of the observations, although they may be broadened slightly by nebulosity associated with SVS 13. Similar profile plots were produced for the CO 2-0 bandhead and Br $\gamma$  line emission (not shown).

Only one component is evident in each of the CO, Br $\gamma$  and [Fe II] profiles, while as many as five separate peaks are identified in the H $_2$  profile (labeled in Figure 4). From Lorentzian

fitting, the offsets with respect to the source continuum position and the FWHM of the individual components seen in each line were measured. These are given in Table 1. The CO and Br $\gamma$  peaks are unresolved and are precisely coincident, to within a few AU, with the source continuum; we see no evidence for CO or H $\alpha$  components associated with the outflow.

The [Fe II] profile is, on the other hand, marginally resolved. In the echelle data of Davis et al. (2003) and Takami et al. (2005) a radial velocity of  $\sim 140 \text{ km s}^{-1}$  with respect to the systemic velocity was assigned to this component. Presumably this compact, high-velocity emission derives from a discrete knot or shock front near the base of the jet, rather than from an extended emission region.

In the H $_2$  data, we see an interesting trend where the size (FWHM) of each component increases with distance from the source (Table 1). Moreover, if the H $_2$  and [Fe II] trace the same jet material, this trend extends to the [Fe II] data; the closer a component is to the source continuum, the less extended it appears to be. The H $_2$  components also decrease in intensity with distance. This behavior could be explained by the cooling, decreased excitation and expansion of “packets” of gas as they travel away from the source. A decrease in gas density and excitation temperature is inferred from the excitation analysis of Takami et al. (2005). A similar trend is also seen in small-scale jets from T Tauri stars (Bacciotti et al. 2000; Woitas et al. 2002).

Directly behind a fast-moving shock the very hot ( $T \sim 10^3 - 10^5 \text{ K}$ ) post shock gas will radiatively cool very rapidly, before the region has time to expand. However, the bulk of the material in the gas packet, *behind* the shock front working surface, may expand adiabatically. If the pressure inside the warm ( $T \sim 100 \text{ K}$ ) gas packet approaches that of the surrounding medium as it expands, decreasing by a factor of  $\sim 10$ -100, and if at the same time the gas temperature in the packet decreases by a factor of 3-10 as it travels a distance of a few arcseconds (equivalent to the inter-knot spacing), then the packet might be expected to increase in volume by a factor of 1-30, or in diameter by a factor of 1-3. Isothermal expansion would result in greater expansion, while a lower pressure gradient would suppress expansion. Either way, the ratio is potentially consistent with the relative sizes of the H $_2$  components in Table 1.

#### 4. Proper Motions

By comparing the *VLT* data with the earlier *Subaru* observations of Takami et al. (2005) we can measure, or at least set upper limits on, the proper motions (PMs) of the [Fe II] and H $_2$  components. The *Subaru* observations, although at higher spectral resolution ( $R \sim 1.1 \times 10^4$ ),

were not obtained with AO correction. However, the *Subaru* pixel scale ( $0.060''(\pm 0.002'')$ ) does fully sample the seeing and the same slit position angle ( $159^\circ$ ) was used with both instruments. Offsets of emission features along the jet axis can therefore be measured accurately and a direct comparison made between the *VLT* and *Subaru* observations (see Table 2). Note, however, that the *Subaru* slit was slightly wider than the *VLT* slit;  $0.30''$  versus  $0.172''$ .

- In the *VLT* H-band observations, the single [Fe II] component in Figure 4 may correspond to the high-velocity peak seen in the *Subaru* data, for which Takami et al. (2005) assign a radial velocity of  $\sim 140 \text{ km s}^{-1}$ . Gaussian fitting yields an offset of  $0.10''(\pm 0.01'')$  for the *Subaru* peak. Curiously, the offset of the *VLT* peak in Table 2 implies that this feature has moved upwind, i.e. *closer* to the source. We certainly see no evidence for pronounced movement away from the jet source.
- In the *Subaru* K-band echelle data two velocity components are resolved in  $\text{H}_2$ ; a bright, low-velocity component (LVC) blue-shifted by  $\sim 30 \text{ km s}^{-1}$  that is spatially offset along the jet by  $0.23''(\pm 0.01'')$ , and a fainter, more diffuse, high-velocity component (HVC) blue-shifted by  $\sim 100 \text{ km s}^{-1}$  that is offset by  $1.27''(\pm 0.02'')$ . These two peaks, which are spatially as well as kinematically separate, probably correspond to the first two components in Figure 4. In Figure 5 we compare the *Subaru* data with smoothed *VLT* data: here the components clearly have a similar spatial offset, width and brightness ratio. (Note that if the data were normalized to the HVC/component 2 peak, then the *Subaru* LVC would be brighter than the *VLT* component 1. Given the wider *Subaru* slit, one would expect this to be the case if the LVC traced a broader flow component than the HVC.) For the LVC/component 1, the offsets in Table 2 indicate a shift downwind of  $0.06''(\pm 0.02'')$  over the 783 day time interval between the *Subaru* and *VLT* observations. However, the HVC/component 2, like the high-velocity [Fe II] component, again exhibits no measurable PM away from the source.

From the radial velocities of the HVC and LVC, and assuming an inclination angle of  $40^\circ$  to the line of sight and a distance of 300 pc to SVS 13, then over the time period between the observations the  $\text{H}_2$  LVC and HVC should have moved by  $0.04''$  (12 AU) and  $0.13''$  (38 AU) on the sky, while the [Fe II] feature should have moved by  $0.18''$  (53 AU). Clearly, only the  $\text{H}_2$  LVC has a PM consistent with the observed radial velocity. Such consistency is expected if, for example, the gas is accelerated by a fast-moving shock front in a heavy jet.

The apparent lack of movement of the  $\text{H}_2$  HVC could result from: (1) the larger errors associated with the positional measurements of this fainter, more extended feature; (2) blending of component 2 with component 3 (Table 1) in the lower-spatial-resolution *Subaru* data, so that the overall peak appears shifted downwind; or (3) the fact that the time

interval between the observations is comparable to the molecular cooling time and therefore the timescale for morphological change, which could introduce unknown errors on the PM measurements.

The lack of a measurable PM in the [Fe II] peak is more difficult to explain. If the [Fe II] peak was associated with ejected clumps or bullets, then one would perhaps expect to see additional components along the flow axis (as is the case in H<sub>2</sub>). Instead, the [Fe II] is confined to a single, very compact peak at the jet base. The [Fe II] could be associated with a stationary, collimating shock, similar to that described in the models of Ouyed & Pudritz (1994). If this is indeed the case, the collimation point would be at a distance of  $\sim 20$  AU from the source.

On the other hand, we may be observing two completely independent [Fe II] peaks in the *Subaru* and *VLT* data, rather than the same near-stationary feature. The *Subaru* feature may have faded, to be replaced by a new peak in the *VLT* observations. The cooling time, from 20,000 K to 7,000 K for dense ( $10^5 - 10^6$  cm<sup>-3</sup>), post-shock gas will be of the order of weeks or even days (Smith 2003), so morphological changes are certainly possible. This might explain the apparent “upwind” movement of this feature.

A number of groups have attempted to *image* the emission-line region at the base of the SVS 13 outflow. Davis et al. (2002) used a Fabry-Perot (FP) etalon to “boost” the line/continuum ratio in their data. The H<sub>2</sub> emission at the jet base is certainly evident in their image, although the poor spatial resolution of their observations ( $\sim 1''$ ) somewhat limits their ability to extract spatial information. They do collapse their image along an axis perpendicular to the jet and attempt to subtract the continuum emission from the resulting profile (their Figure 4). They identify a “peak” and a “plateau” along the jet axis which may correspond to H<sub>2</sub> components 2 and 3 in the *VLT* data. We list the offsets of these features in Table 2.

Noriega-Crespo et al. (2002) used the *HST* to obtain high-spatial resolution near-IR images of the HH 7-11 outflow. They present a continuum-subtracted H<sub>2</sub> image of SVS 13 (their Figure 3). However, residual artifacts left over from the continuum subtraction, in the bright core but also in a ring of radius  $\sim 1''$ , make identifying features within  $0.5-1.0''$  of SVS 13 more-or-less impossible. However, they do detect and resolve the H<sub>2</sub> emission in the flow at offsets of  $>1''$ . Within  $1''-2''$  of SVS 13 the H<sub>2</sub> appears to comprise at least two knots superimposed on to a patch of moderately extended emission, suggesting a broad opening angle for the H<sub>2</sub> flow. Component 2 in the *VLT* data (the HVC in the *Subaru* observations) may therefore constitute *two knots*; we give a combined offset for these two features (measured along the *VLT/Subaru* slit axis) in Table 2 for reference.

Overall, the results from these two imaging surveys can only be used to confirm the presence of emission features. Uncertainties in the continuum subtraction limit their usefulness when measuring PMs. Notably, the compact LVC evident in both the *Subaru* and *VLT* spectroscopy was not extracted from the FP or *HST* images.

Clearly, follow-up observations with the *NACO* system are needed to better constrain the PM measurements discussed above, particularly for the [Fe II] peak and the H<sub>2</sub> components further downwind. Confirmation of the “stationary” [Fe II] peak would add credence to the collimation-shock interpretation. If we also ultimately find that the H<sub>2</sub> peaks do *not* move, then in H<sub>2</sub> we could be witnessing a warm, stationary region or perhaps a turbulent mixing layer between the jet and ambient medium at the jet base through which jet material flows, rather than discrete bullets or clumps ejected during episodes of increased accretion. However, given the tentative result for the LVC, and the fact that knots in Herbig-Haro jets and molecular flows typically do have large proper motions (Reipurth & Bally 2001), for H<sub>2</sub> at least, this seems unlikely.

Finally, we mention that the dynamical age of the H<sub>2</sub> LVC, components 1 in the *VLT* data, when derived from its PM and offset in Table 1, is  $\sim 10$  yrs. Notably, the optical outburst reported by Eislöffel et al. (1991) occurred roughly 15 yrs before the observations reported here. Our results are thus reasonably consistent with the H<sub>2</sub> LVC being produced by this outburst and the associated increase in accretion.

## REFERENCES

- Bacciotti, F., Mundt, R., Ray, T.P., Eislöffel, J., Solf, J., & Camenzind, M. 2000, ApJ, 537, L49
- Bachiller, R., Gueth, F., Guilloteau, S., Tafalla, M., & Dutrey A. 2000, A&A, 362, L33
- Cernis, K. 1990, Ap&SS, 166, 315
- Chrysostomou, A., Hobson, J., Smith, M.D., Davis, C.J., & Berndsen, A. 2000, MNRAS, 314, 229
- Davis, C.J., Ray, T.P., Desroches, L., & Aspin, C. 2001, MNRAS, 326, 524
- Davis, C.J., Stern, L., Ray, T.P., & Chrysostomou, A. 2002, A&A, 382, 1021
- Davis, C.J., Whelan, E., Ray, T.P., & Chrysostomou, A. 2003, A&A, 397, 693



- Eislöffel, J., Guenther, E., Hessman, F.V., Mundt, R., Poetzel, R., Carr, J.S., Beckwith, S.V., & Ray T.P. 1991, A&A, 393, L19
- Hartigan, P., Raymond, J.C., & Hartmann, L. 1987, ApJ, 316, 323
- Nisini, B., Bacciotti, F., Giannini, T., Massi, F., Eislöffel, J., Podio, L., & Ray, T.P. 2005, A&A, 441, 159
- Noriega-Crespo, A., Cotera, A., Young, E., & Chen, H. 2002, ApJ, 580, 959
- Ouyed, R., & Pudritz, R.E 1994, ApJ, 423, 753
- Pyo, T-S., Hayashi, M., Kobayashi, N., Terada, H., Goto, M., Yamashita, T., Tokunaga, A.T., & Itoh, Y. 2002, ApJ, 570, 724
- Reipurth, B., & Bally, J. 2001, ARA&A, 39, 403
- Smith, M.D. 2003, Ap&SS, 287, 195
- Smith, M.D., Khanzadyan T., & Davis, C.J. 2003, MNRAS, 339, 524
- Takami, M., Chrysostomou, A., Ray, T.P., Davis, C.J., Dent, W.R.F., Bailey, J., Tamura, M., Terada, H., & Pyo T.S. 2005, ApJ, submitted
- Vacca, W.D., Cushing, M.C., & Rayner, J.T. 2003, PASP, 115,389
- Whelan, E., Ray, T.P., & Davis, C.J., 2004 A&A, 417, 247
- Woitas, J., Ray, T.P., Bacciotti, F., Davis, C.J., & Eislöffel, J. 2002, ApJ, 540, 336
- de Zeeuw, P.T., Hoogerwerf, R., de Bruijine, J.H.J., Brown, A.G.A., & Blaauw, A. 1999, AJ, 117, 354.

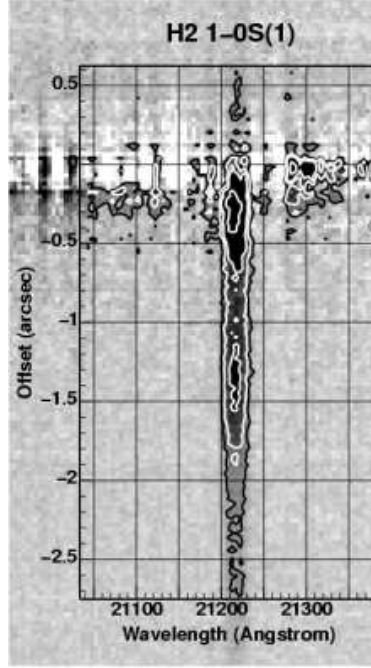


Fig. 1.— Contour plot extracted from the K-band spectral image showing the H<sub>2</sub> 1-0S(1) emission. Negative offsets are along the south-eastern, blue-shifted jet axis. The continuum associated with SVS 13 has been fitted and removed (see text).

Table 1: Parameters from the profile fitting

Line <sup>a</sup>	Offset (arcsec)	Offset (AU)	FWHM (arcsec)
H <sub>2</sub> - 1	0.29(±0.009)	87.8(±3)	0.44
H <sub>2</sub> - 2	1.19(±0.018)	358(±6)	1.3
H <sub>2</sub> - 3	2.0(±0.1)	600(±30)	1.5
H <sub>2</sub> - 4	4.8(±0.2)	1428(±30)	1.8
H <sub>2</sub> - 5 <sup>b</sup>	0.28(±0.1)	86(±30)	1.0
[FeII]	0.061(±0.004)	18.3(±1.2)	0.29
Brγ	0.001(±0.003)	<0.9	0.19
CO	0.004(±0.003)	<1.2	0.17

<sup>a</sup>Lorentzian fits to five components in H<sub>2</sub> (see Figure 4); a single Lorentzian is fitted to the single peak in each of the extracted CO, [Fe II] and Brγ profiles.

<sup>b</sup>Possible component in the red-shifted counterflow (positive offsets in Figure 4).

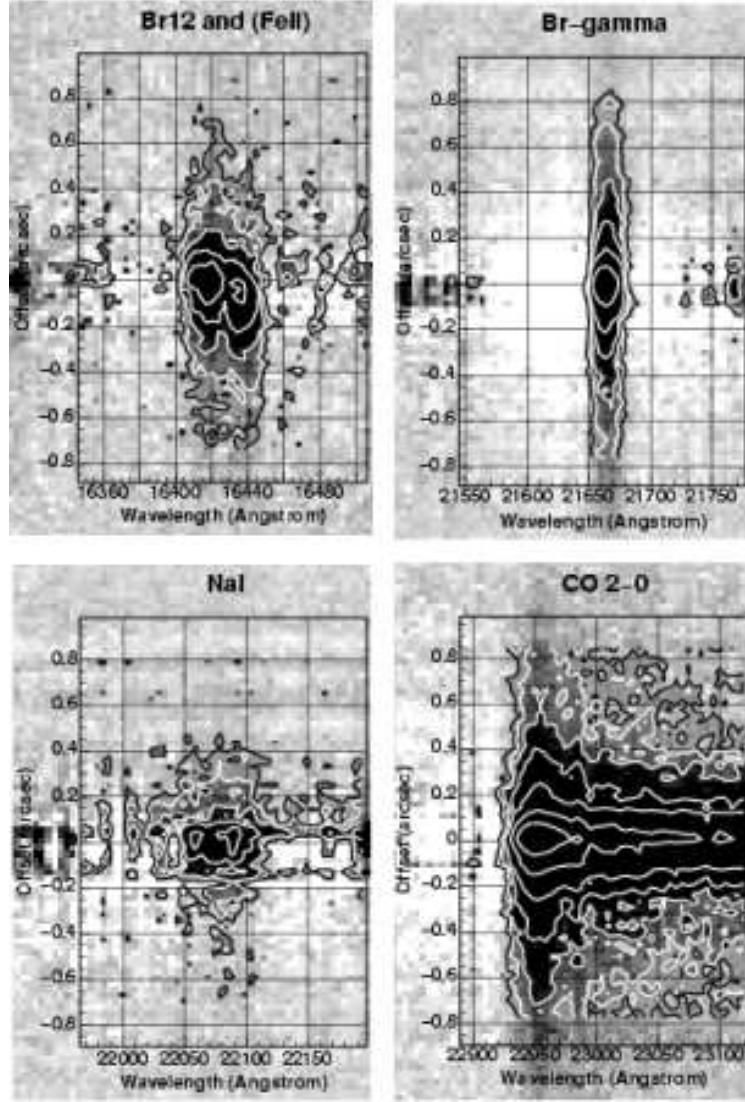


Fig. 2.— Contour plots extracted from the H- and K-band spectral images showing emission in select lines. The continuum has again been removed.

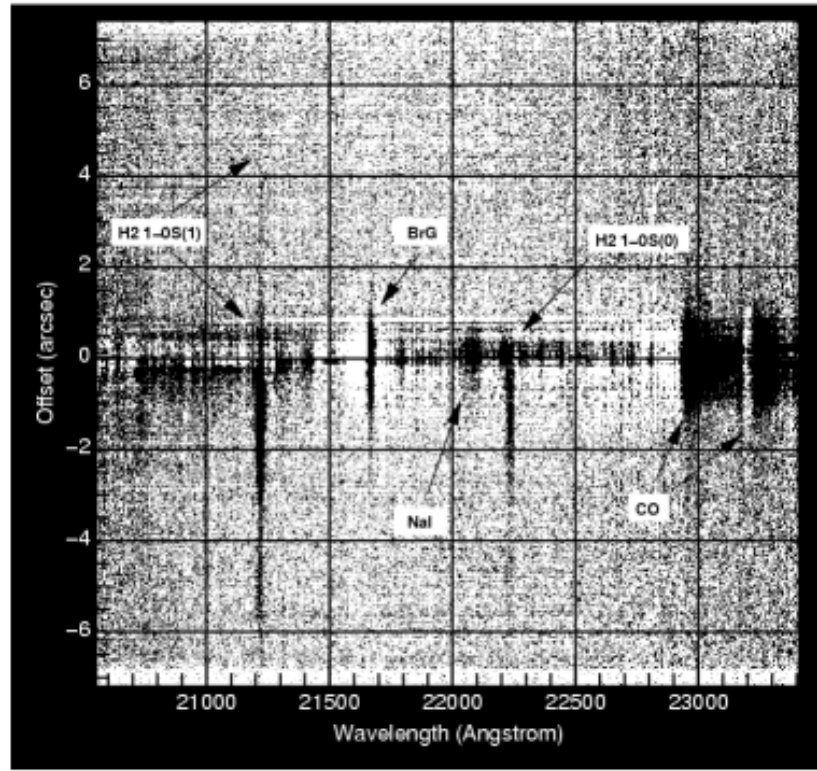


Fig. 3.— Continuum-subtracted K-band spectral image with a grey-scale stretch set to show the faint  $\text{H}_2$  emission along the slit.

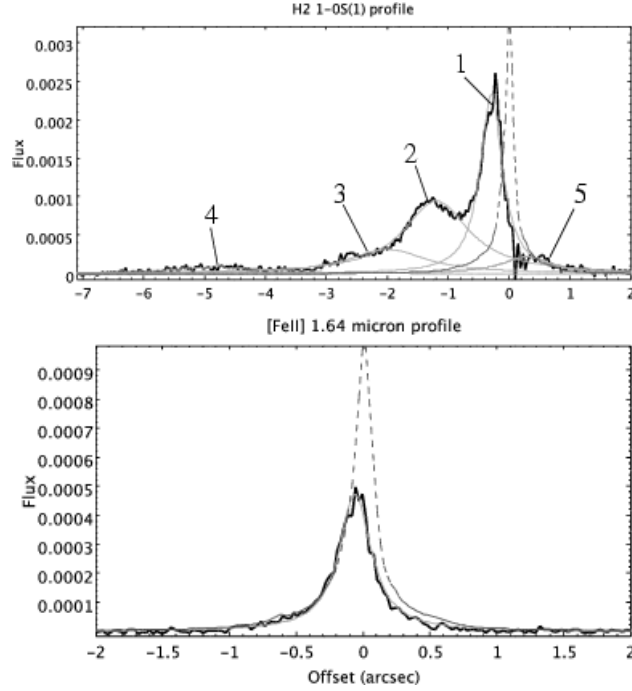


Fig. 4.— Profile plots showing the distribution of  $\text{H}_2$  1-0S(1) and  $[\text{Fe II}]$  1.644  $\mu\text{m}$  emission along the slit. The fine grey lines show Lorentzian fits to the data; one fit for the  $[\text{Fe II}]$  peak though five fits to the  $\text{H}_2$  data. The dashed line shows the profile through the continuum adjacent to each line.

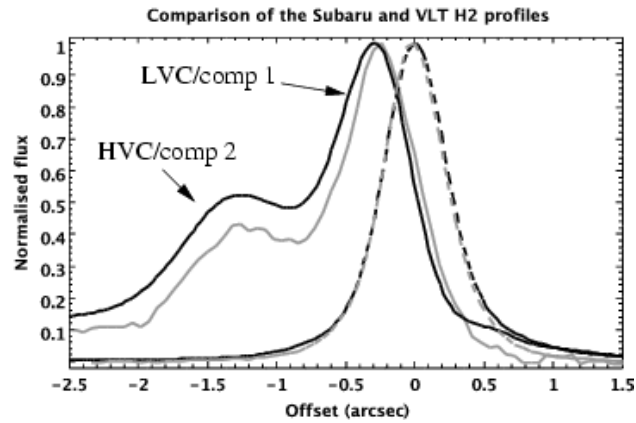


Fig. 5.— Comparison of the *Subaru* (Grey) and *VLT* (black)  $\text{H}_2$  profiles. The dashed lines show the adjacent continuum data. The *VLT* observations have been Gaussian-smoothed to the spatial resolution of the *Subaru* data.

Table 2: Component offsets and proper motions

Line/component <sup>a</sup>	<i>VLT</i> <sup>b</sup> Offset (")	<i>Subaru</i> <sup>c</sup> Offset (")	<i>UKIRT</i> <sup>d</sup> Offset (")	<i>HST</i> <sup>e</sup> Offset (")	P.M. <sup>f</sup> ("/yr)
H <sub>2</sub> - 1	0.29(±0.009)	0.23(±0.01)	...	...	0.028(±0.007)
H <sub>2</sub> - 2	1.19(±0.018)	1.27(±0.02)	1.28(±0.01)	~1.1(±0.5) <sup>g</sup>	<0.05
H <sub>2</sub> - 3	2.0(±0.1)	–	2.13(±0.09)	...	<0.03
H <sub>2</sub> - 4	4.8(±0.2)	–	...	...	...
[FeII]	0.061(±0.004)	0.10(±0.01)	...	...	-0.018(±0.006)

<sup>a</sup>Same as Table 1.

<sup>b</sup>*VLT* spectroscopy presented in this paper; data obtained on 1/17/2005.

<sup>c</sup>*Subaru* spectroscopy presented in Takami et al. (2005); data obtained on 11/25/2002.

<sup>d</sup>*UKIRT* Fabry-Perot imaging from Davis et al. (2002); data obtained on 11/23/2000.

<sup>e</sup>*HST-NICMOS* imaging from Noriega-Crespo et al. (2002); data obtained on 1/9/1998.

<sup>f</sup>Proper motion measurements or upper limits; the negative value for the [Fe II] 1.644  $\mu\text{m}$  peak reflects its apparent motion *towards* the source.

<sup>g</sup>Multiple components spread over an area of roughly 1".